Low-energy total and differential cross sections for the electron-impact excitation of Si^{2+} and Ar^{6+}

D. C. Griffin
Department of Physics, Rollins College, Winter Park, Florida 32789

M. S. Pindzola and N. R. Badnell
Department of Physics, Auburn University, Auburn, Alabama 36849
(Received 8 October 1992; revised manuscript received 17 December 1992)

The total and angular differential excitation cross sections for the transitions $3s^2\,{}^1S \rightarrow 3s3p\,{}^3P$, $3s^2\,{}^1S \rightarrow 3s3p\,{}^1P$, and $3s3p\,{}^3P \rightarrow 3s3p\,{}^1P$ in the Mg-like ions Si^{2+} and Ar^{6+} are determined in the threshold energy region using the close-coupling R-matrix method. The total cross sections for all three transitions in both ions exhibit strong resonance structures near threshold. We focus our analysis on the angular distribution of the scattered electrons. The differential cross sections are found to undergo rapid and strong variations when the incident energy is tuned through the autoionizing resonance transitions. In Ar^{6+}, we also examine the angular distribution of the scattered electrons associated with the nonresonant background cross sections for the two transitions from the ground state. For the dipole-allowed transition, the electrons are preferentially backscattered near the excitation threshold; however, the fraction of electrons scattered in the forward direction increases dramatically with energy. The corresponding behavior for the spin-forbidden transition is quite different. We discuss the implications of these results to possible excitation measurements in which the scattered electrons are collected.

PACS number(s): 34.80.Kw

I. INTRODUCTION

The recent development of both crossed-beam experiments [1–3] to measure fixed-angle differential cross sections and merged-beam experiments [4,5] to measure integrated-angle total cross sections promises to provide interesting tests of the theoretical many-body methods used to calculate electron-ion excitation processes. Although the number of theoretical calculations of angle-dependent cross sections in electron-atom collisions is vast [6], due mainly to the many detailed experimental studies, there have been relatively few calculations of differential excitation cross sections in electron-ion collisions [7–10]. However, since information regarding the angular distribution of electrons is needed for the proper interpretation of the new generation of electron-ion experiments which collect the scattered electrons, it is important to consider not only total excitation cross sections for multiply charged ions, but also angular differential cross sections.

In this paper we present low-energy excitation cross sections, obtained using the close-coupling R-matrix method for the three transitions $3s^2\,{}^1S \rightarrow 3s3p\,{}^3P$, $3s^2\,{}^1S \rightarrow 3s3p\,{}^1P$, and $3s3p\,{}^3P \rightarrow 3s3p\,{}^1P$ in the Mg-like ions Si^{2+} and Ar^{6+}. These cases were chosen because of the interesting and dominant resonance structure in the threshold region for the spin-forbidden transition $3s^2\,{}^1S \rightarrow 3s3p\,{}^3P$ in Si^{2+}, observed in earlier calculations on this ion [11], and because of possible excitation measurements for these ions in the threshold region [12].

In Si^{2+}, a 12-state close-coupling calculation is performed similar to that of Baluja, Burke, and Kingston [11], while in Ar^{6+}, comparable accuracy is obtained from a smaller 8-state close-coupling expansion. Using these results, we find that the angular distribution of scattered electrons is strongly influenced by the pronounced resonance structures in the threshold region for all three transitions in both ions. In addition, for the two transitions from the $3s^2\,{}^1S$ ground state in Ar^{6+}, we eliminate the resonance contributions by performing simple 2-state calculations. In this way we study the angular distribution of scattered electrons associated with the background cross sections and find that the variation in angular scattering with electron energy for the dipole-allowed transition is quite different from that of the spin-forbidden transition. The importance of these results to possible merged-beam experiments is discussed.

The remainder of this paper is arranged as follows: In Sec. II we give a summary of the theoretical methods employed. In Sec. III we discuss the details of the numerical calculations, present results for both total and angular differential cross sections, and analyze the angular distribution of the scattered electron. Finally in Sec. IV, we provide a brief summary of the results and their implications.

II. THEORETICAL METHODS

The R-matrix method [13] provides an efficient means for solving the close-coupling equations. This method is especially advantageous for calculating electron-impact excitation cross sections for transitions where strong resonance structures are present and a large number of energies is required to resolve these structures. For this work we employed the R-matrix programs developed for the Opacity Project [14].

In these calculations the latest set of Fischer's multiconfiguration-Hartree-Fock (MCHF) programs [15]

was used to generate the bound radial orbitals. Like a number of other programs used to calculate bound-state radial wave functions, these codes allow for the generation of nonspectroscopic pseudo-orbitals. Such orbitals can be used to represent configuration interaction with a large number of highly excited configurations, through the inclusion of a relatively small number of pseudostates. In addition, scattering calculations normally require a unique set of radial wave functions for all configurations included in the basis expansion, yet, especially in low-charge-state ions, such wave functions can vary significantly from one configuration to the next. The addition of states containing pseudo-orbitals to the basis-set expansion can be used to represent such orbital relaxation effects.

A primary emphasis in the present work is the use of differential cross sections to determine the angular distribution of scattered electrons. In LS coupling, the angular differential cross section for excitation from an initial term $\alpha_i L_i S_i$ to a final term $\alpha_f L_f S_f$ is given by

$$\frac{d\sigma_{if}}{d\Omega}=\frac{1}{8(2L_i+1)(2S_i+1)k_i^2}\times\sum_{\lambda}(2\lambda+1)\left[\sum_{l_i,l_f,l_i',l_f'}\begin{bmatrix} l_i & l_i' & \lambda \\ 0 & 0 & 0\end{bmatrix}\begin{bmatrix} l_f & l_f' & \lambda \\ 0 & 0 & 0\end{bmatrix} i^{(l_i-l_f)}i^{(l_f'-l_i')}e^{i(\sigma_{l_i}-\sigma_{l_i'}+\sigma_{l_f}-\sigma_{l_f'})}\times\sum_{j_t}(-1)^{j_t+\lambda}(2j_t+1)\begin{Bmatrix} l_i & l_f & j_t \\ l_f' & l_i' & \lambda\end{Bmatrix}\sum_{S}M^*(\beta_i l_i'\beta_f l_f' j_t S)M(\beta_i l_i\beta_f l_f j_t S)\right]P_\lambda(\cos\theta)\ , \quad (1)$$

where k_i is the linear momentum of the incident electron; l_i and l_f are the orbital angular momenta of the incident and scattered electrons, respectively; σ_l is the Coulomb phase shift; and β is employed to represent the quantum numbers αLS associated with each term. The sums are performed over the multipolar-expansion parameter λ; the free-electron angular momenta l; the momentum-transfer quantum number j_t employed by Salvini [16]; and the total-spin quantum number S of the $(N+1)$-electron system. Finally, the function $M(\beta_i l_i\beta_f l_f j_t S)$ is defined by the equation

$$M(\beta_i l_i\beta_f l_f j_t S)=\sum_{\pi,L}(-1)^{l_i+l_f}[(2l_i+1)(2l_f+1)(2S+1)]^{1/2}\times(-1)^L(2L+1)\times\begin{Bmatrix} L_i & L_f & j_t \\ l_f & l_i & L\end{Bmatrix}T^{LS\pi}_{l_i l_f}(\beta_i\rightarrow\beta_f)\ , \quad (2)$$

where π and L are the parity and total angular momentum of the $(N+1)$-electron system and T is an element of the **T** matrix, which is related to the **S** matrix and the **K** matrix by the equation

$$\mathbf{T}=\mathbf{1}-\mathbf{S}=-\frac{2i\mathbf{K}}{(\mathbf{1}-i\mathbf{K})}\ . \quad (3)$$

In this case, the **K** matrix is generated from the R-matrix programs. The differential cross sections were calculated using a program we developed [9], which is similar to the one written earlier by Salvini [16].

In addition to differential cross sections, it is also useful to consider the partial angular cross section $\sigma_p(\theta_f)$, which from 0 to a final angle θ_f is defined by the equation

$$\sigma_p(\theta_f)=2\pi\int_0^{\theta_f}\frac{d\sigma}{d\Omega}\sin\theta\, d\theta\ . \quad (4)$$

We can then define the partial-cross-section fraction as the partial angular cross section divided by the total cross section. As will be seen, these fractions are quite useful in analyzing the angular distribution of scattered electrons.

III. RESULTS

In earlier work, Baluja, Burke, and Kingston [11] determined the collision strength for the $3s^2\,{}^1S\rightarrow 3s3p\,{}^3P$ spin-forbidden transition in Si^{2+} and in [17] they determined effective collision strengths, averaged over a Maxwellian distribution of electrons, for transitions among the 12 lowest terms of this ion. For these calculations, they used scattering matrices generated from a 12-state R-matrix close-coupling calculation, which employed an elaborate set of configuration-interaction target wave functions determined by Baluja and Hibbert [18]; their bound-state basis set was found to provide energies in good agreement with experimental values, and also length and velocity oscillator strengths which are close to each other, as well as those of Victor, Stewart, and Laughlin [19]. In order to generate total and differential cross sections for the transitions among the lowest three terms of Si^{2+}, we have performed similar calculations.

The orbitals and configuration-interaction expansions used to generate the bound-state wave functions, which were used in the calculations for Si^{2+} reported here, are described in Table I. With the exception of the $4\bar{d}$, $4\bar{f}$, and $5\bar{s}$ pseudo-orbitals, all other orbitals are spectroscopic and were generated from single-configuration-Hartree-Fock (SCHF) calculations; the pseudo-orbitals were determined from a set of MCHF calculations. We also generated another basis set identical to the one described in Table I, except that no pseudo-orbitals were employed and the $4d$, $4f$, and $5s$ orbitals were generated from SCHF calculations for the $3s4d\ {}^1D$, $3s4f\ {}^1F$, and $3s5s\ {}^1S$ terms, respectively. We settled on the use of the orbital set described in Table I, primarily because it provided better agreement with the experimental energies for the

TABLE I. Configuration-interaction expansions for 12-state R-matrix close-coupling calculations in Si^{2+} (69 terms). The $1s$, $2s$, $2p$, and $3s$ orbitals were generated from a SCHF calculation for the term $3s^2\,{}^1S$, while the $3p$, $3d$, $4s$, and $4p$ orbitals were generated from SCHF calculations for the terms $3s3p\,{}^1P$, $3s3d\,{}^1D$, $3d4s\,{}^1S$, and $3s4p\,{}^1P$, respectively, with all other orbitals frozen. The $4\bar{d}$ pseudo-orbital was determined from a MCHF calculation for ${}^1S_e$ (not including the $4\bar{f}^2$ or $4s5\bar{s}$ configurations), with all other orbitals frozen; the $4\bar{f}$ pseudo-orbital was determined form a MCHF calculation for ${}^1D_e$ (not including the $3d5\bar{s}$ configuration), with all other orbitals frozen; and the $5\bar{s}$ pseudo-orbital was determined from a MCHF calculation for ${}^1P_o$, with all other orbitals frozen. The $5\bar{s}$ pseudo-orbital was employed to partially correct the $3snl$ states for the difference between the $3s$ orbital in $3s^2$ and $3snl$.

$SL\Pi$	Configurations
${}^1S_e$	$3s^2$, $3p^2$, $3d^2$, $3s4s$, $3p4p$, $3d4\bar{d}$, $4s^2$, $4p^2$, $4\bar{d}^2$, $4\bar{f}^2$, $4s5\bar{s}$
${}^3S_e$	$3s4s$, $3p4p$, $3d4\bar{d}$, $4s5\bar{s}$
${}^{1,3}P_o$	$3s3p$, $3p3d$, $3s4p$, $3p4s$, $3p4\bar{d}$, $3d4p$, $3d4\bar{f}$, $3p5\bar{s}$, $4s4p$, $4p4\bar{d}$, $4\bar{d}4\bar{f}$, $4p5\bar{s}$
${}^1D_e$	$3s3d$, $3p^2$, $3d^2$, $3s4\bar{d}$, $3p4p$, $3p4\bar{f}$, $3d4s$, $3d4\bar{d}$, $3d5\bar{s}$, $4s4\bar{d}$, $4p^2$, $4p4\bar{f}$, $4\bar{d}^2$, $4\bar{f}^2$
${}^3D_e$	$3s3d$, $3d4\bar{d}$, $3p4p$, $3p4\bar{f}$, $3d4s$, $3d4\bar{d}$, $3d5\bar{s}$, $4s4\bar{d}$, $4p4\bar{f}$
${}^3P_e$	$3p^2$, $3d^2$, $3p4p$, $3d4\bar{d}$, $4p^2$, $4\bar{d}^2$, $4\bar{f}^2$

$3s3p\,{}^1P$ term, as well as the $3s3d\,{}^1D$ term.

Configuration-interaction expansions involving the 69 LS terms listed in Table I resulted in the energies for the lowest 12 terms of this ion shown, in comparison to the experimental energies [20], in Table II. These are the 12 terms that were employed in the close-coupling expansion for the scattering problem. As can be seen, the agreement with experiment is, in general, quite good and comparable to the results obtained by Baluja and Hibbert [18]. In Table III we show the results for length and velocity oscillator strengths for the same transitions between those terms considered in Ref. [18]. The agreement between the length and velocity values is quite good for transitions from $3s^2\,{}^1S$, $3s3p\,{}^3P$, and $3s3p\,{}^1P$, and the oscillator strengths from these terms are similar to those obtained by Baluja and Hibbert [18]. Transitions from the higher terms are not as satisfactory; however, since we are interested in the electron-impact excitation between the lowest three terms, this should not present a serious problem.

In the close-coupling R-matrix calculations presented here, we included, in the bound-channel part of the close-coupling expansion, the $(N+1)$-electron terms which could be constructed by adding all orbitals to all 69 terms included in the N-electron configuration-interaction expansions, rather than just those that could be constructed from the 12 terms included in the close-coupling expansion. This is often done in close-coupling calculations in order to increase the correlation within the $(N+1)$-electron problem. Indeed, a comparison of calculations with and without this extra correlation demonstrated the sensitivity of the resonance structure to its inclusion. When the configuration-interaction expansions include pseudo-orbitals, as they do here, this procedure leads to pseudoresonances; however, these were found to occur high above the energy range of interest.

Partial waves up to a total angular momentum of 12 were included in our calculation, and a top-up procedure was employed for the dipole-allowed transition [21]. As a check on our calculation, we first determined the collision strength for the $3s^2\,{}^1S \rightarrow 3s3p\,{}^3P$ transition and compared it to the collision strength determined by Baluja, Burke, and Kingston [11]. The agreement between these two calculations is excellent with respect to both

TABLE II. Energies (eV) for the terms included in the 12-state close-coupling expansion in Si^{2+} relative to the $3s^2\,{}^1S$ ground state.

Number	Term	Theory	Experiment (Ref. [20])
1	$3s^2\,{}^1S$	0.00	0.00
2	$3s3p\,{}^3P$	6.38	6.56
3	$3s3p\,{}^1P$	10.28	10.28
4	$3p^2\,{}^1D$	14.93	15.15
5	$3p^2\,{}^3P$	15.95	16.10
6	$3s3d\,{}^3D$	17.51	17.72
7	$3s4s\,{}^3S$	18.88	19.02
8	$3p^2\,{}^1S$	19.04	19.03
9	$3s4s\,{}^1S$	19.56	19.72
10	$3s3d\,{}^1D$	20.53	20.55
11	$3s4p\,{}^3P$	21.44	21.73
12	$3s4p\,{}^1P$	21.64	21.88

TABLE III. Absorption oscillator strengths for transitions in Si^{2+}.

Number	Transition	Oscillator strengths Length	Velocity
1	$3s^2\,{}^1S-3s3p\,{}^1P$	1.7099	1.6838
2	$3s^2\,{}^1S-3s4p\,{}^1P$	0.0111	0.0104
3	$3s3p\,{}^3P-3p^2\,{}^3P$	0.5780	0.5715
4	$3s3p\,{}^3P-3s3d\,{}^3D$	0.8966	0.8536
5	$3s3p\,{}^3P-3s4s\,{}^3S$	0.0995	0.0924
6	$3s3p\,{}^1P-3p^2\,{}^1D$	0.0434	0.0482
7	$3s3p\,{}^1P-3p^2\,{}^1S$	0.2630	0.2554
8	$3s3p\,{}^1P-3s4s\,{}^1S$	0.0577	0.0482
9	$3s3p\,{}^1P-3s3d\,{}^1D$	1.8091	1.8117
10	$3p^2\,{}^1D-3s4p\,{}^1P$	0.1452	0.0654
11	$3p^2\,{}^3P-3s4p\,{}^3P$	0.0005	0.0000
12	$3s3d\,{}^3D-3s4p\,{}^3P$	0.1916	0.1017
13	$3s4s\,{}^3S-3s4p\,{}^3P$	1.3144	0.9090
14	$3p^2\,{}^1S-3s4p\,{}^1P$	0.0485	0.0513
15	$3s4s\,{}^1S-3s4p\,{}^1P$	0.8667	0.7876
16	$3s3d\,{}^1D-3s4p\,{}^1P$	0.0423	0.1566

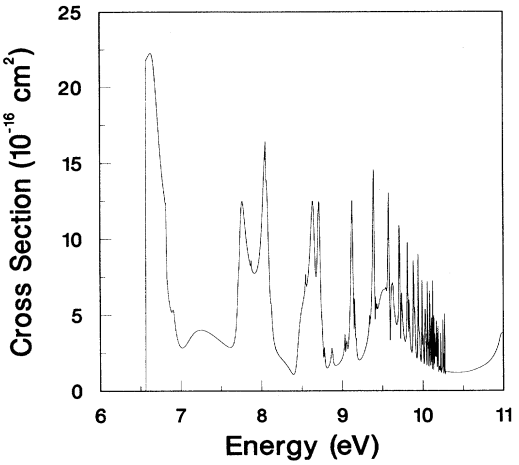

FIG. 1. Cross section for the $3s^2\,{}^1S \rightarrow 3s3p\,{}^3P$ excitation in Si^{2+} from a 12-state R-matrix close-coupling calculation.

the position and the magnitude of the pronounced resonance structures. It is reassuring that, despite the fact that the bound-state wave functions were generated using quite different techniques, and there are some detectable, although small, differences in the energies and oscillators strengths, the collision strengths are nearly identical.

As a further test of the sensitivity of the calculations to the bound-state wave functions, we also determined the total cross sections for the three transitions reported in this paper using our other basis set, which involved only spectroscopic orbitals. Although there were some very slight differences between the two sets of calculations with respect to the position and size of individual resonances, these discrepancies are far too small to have any significant effect on the principal conclusions of this work. The greatest uncertainty with respect to these calculations is probably due to the sensitivity of the resonance structure to the amount of correlation included within the $(N+1)$-electron system, as mentioned in the last paragraph.

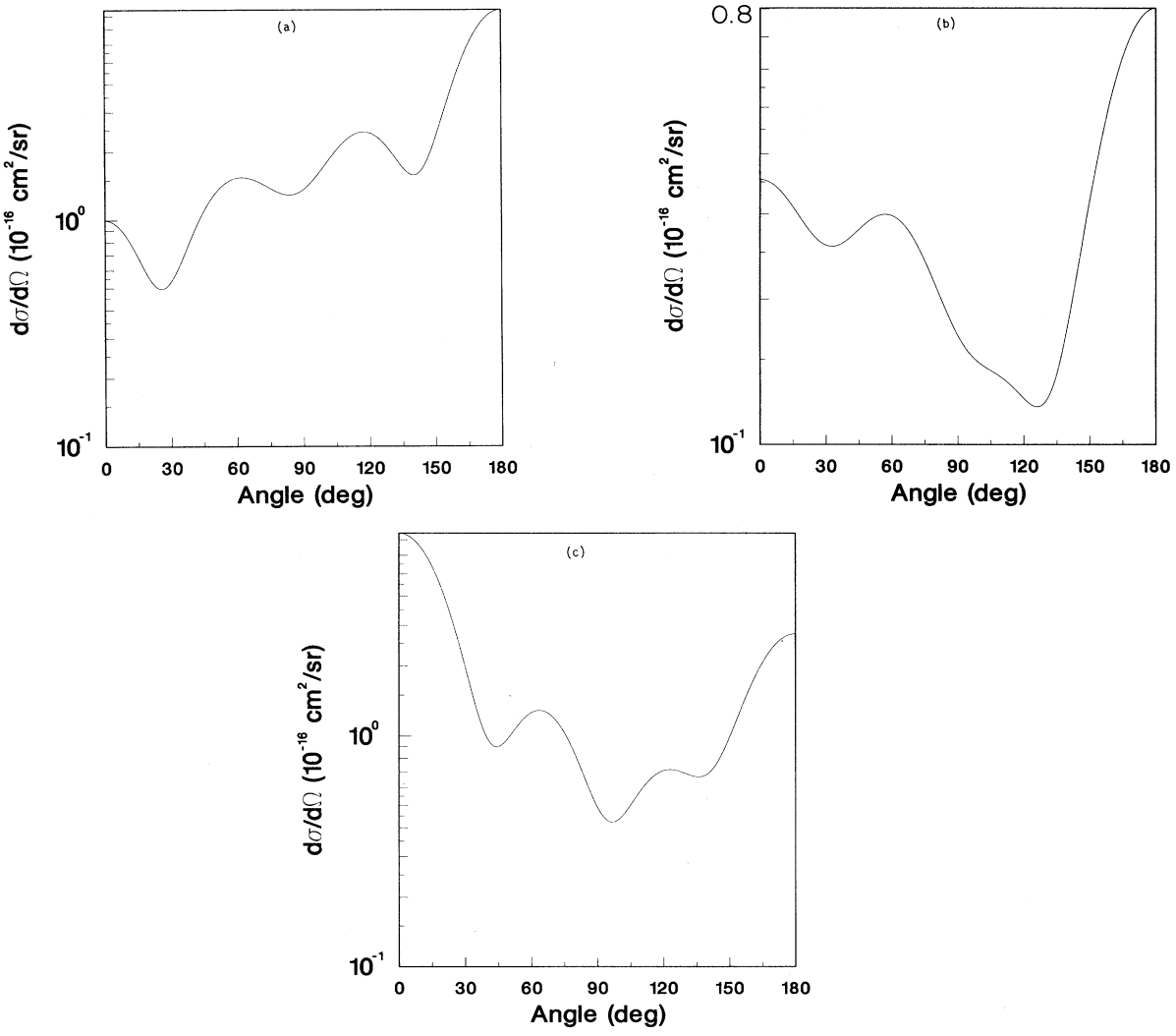

FIG. 2. Angular differential cross sections for the $3s^2\,{}^1S \rightarrow 3s3p\,{}^3P$ excitation in Si^{2+} at energies of (a) 6.6, (b) 7.0, and (c) 8.1 eV.

Our calculated total cross section for the $3s^2\,{}^1S \rightarrow 3s3p\,{}^3P$ transition is shown in Fig. 1. The strong resonance structure in the threshold region was one of the primary reasons for our interest in this particular ion. It presents the opportunity for detailed measurements of these resonances using the merged-beam energy-loss technique [4,5] and such an experiment would provide a much needed test of theory.

However, since these experiments must detect the scattered electrons, knowledge of the angular distribution of the electrons is very important. Therefore, we made a series of differential-cross-section calculations throughout the threshold region. The results for three selected energies are shown in Fig. 2. The first curve corresponds to the peak of the broad resonance near threshold, the second to the dip in the cross section at 7.0 eV, and the third to the large peak, just about 8.0 eV. As can be seen, the variation in the shape of these cross sections is quite pronounced as one moves through the various resonances.

In addition, values of partial-cross-section fractions, defined in Sec. II, are plotted in Fig. 3 as a function of the final angle θ_f for the same energies as those employed in Fig. 2. In the upper portion of Table IV, we also give the partial-cross-section fractions for this transition, corresponding to final angles of 90° and 130° for five energies in the threshold region, including the three energies used to generate Figs. 2 and 3. These plots and the table entries clearly demonstrate how the fraction of electrons scattered through a given range of angles changes dramatically with energy in the resonance region. This should be expected since the angular distribution of Auger electrons emitted from the various $(N+1)$-electron resonant terms will depend on the magnetic states populated during the recombination process.

This variation in scattering angle has important implications for experiments designed to measure electron-impact excitation cross sections in the resonance region. It may be difficult to capture all the scattered electrons in merged-beam energy-loss experiments [4,5] when a large fraction is backscattered in the rest frame of the ion. Nonetheless, measurements of partial cross sections

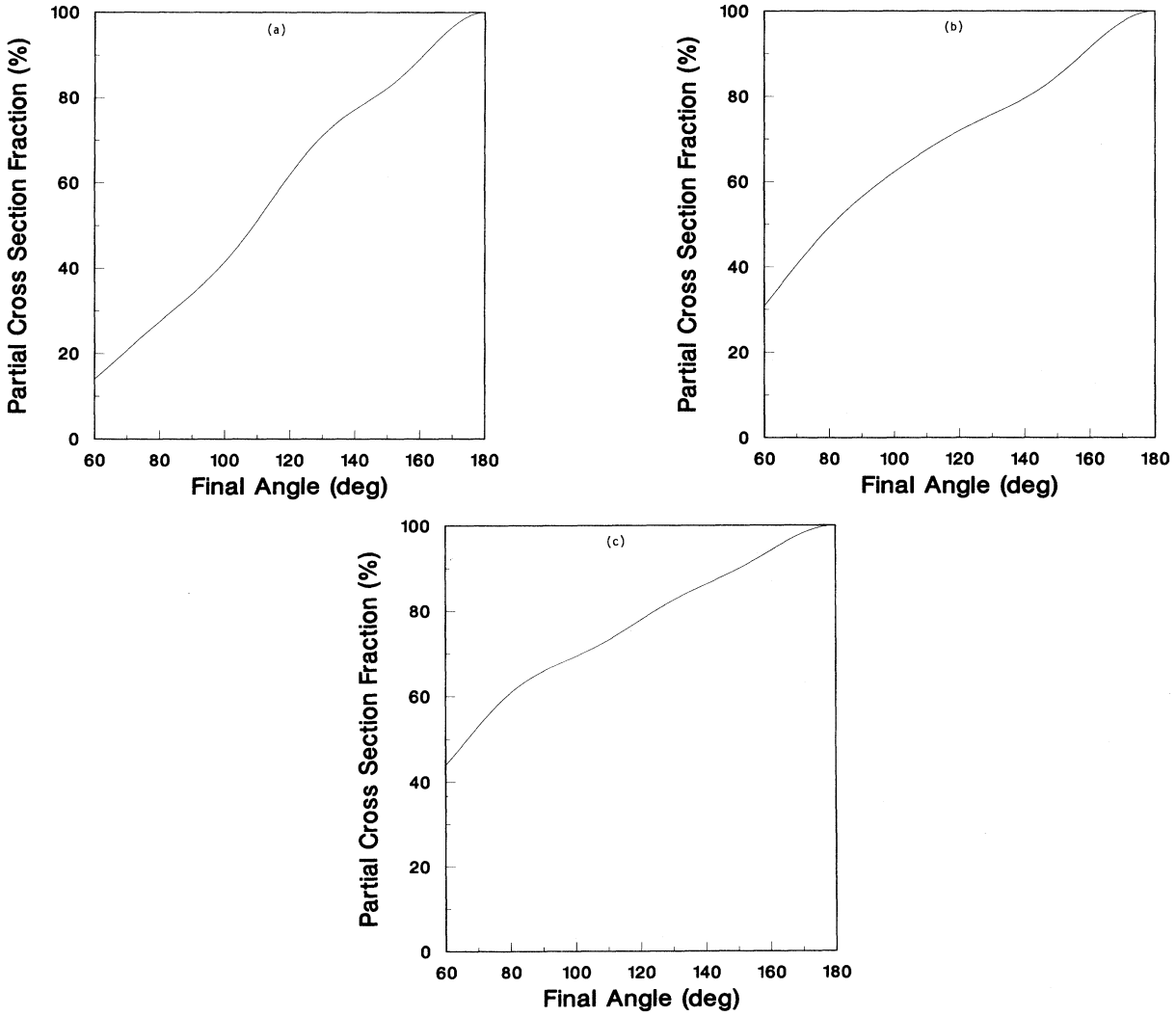

FIG. 3. Partial-cross-section fractions for the $3s^2\,{}^1S \rightarrow 3s3p\,{}^3P$ excitation in Si^{2+} at energies of (a) 6.6, (b) 7.0, and (c) 8.1 eV.

TABLE IV. Partial-cross-section fractions (%) for 12-state R-matrix close-coupling calculation in Si^{2+}.

Transition	Electron energy (eV)	Fraction 0°−90°	Fraction 0°−130°
$3s^2\,{}^1S-3s3p\,{}^3P$	6.6	34.2	71.3
	7.0	56.6	75.9
	7.2	27.0	51.7
	8.1	65.9	82.5
	8.4	55.5	68.4
$3s^2\,{}^1S-3s3p\,{}^1P$	10.3	33.3	66.7
	10.9	38.0	76.4
	11.1	52.0	86.9
	11.7	36.8	54.7
	12.3	57.2	83.6
$3s3p\,{}^3P-3s3p\,{}^1P$	3.8	51.9	67.7
	4.4	56.0	77.0
	4.5	65.3	76.6
	5.1	66.0	85.3
	5.7	47.7	77.9

would also be quite valuable. Their comparison with theoretical partial cross sections would serve as an excellent test of theory and they can be used in conjunction with theoretical partial-cross-section fractions to generate estimates for total cross sections. However, in light of the rapid variations in the angular distributions depicted in Figs. 2 and 3, this is true only if they can be accompanied by precise measurements of the angular range of electrons detected.

In Fig. 4 we show the total cross section for the $3s^2\,{}^1S\rightarrow 3s3p\,{}^1P$ dipole-allowed transition in Si^{2+}. Although the resonance structure is not quite as strong as in the spin-forbidden transition to $3s3p\,{}^3P$, it is still quite pronounced. In addition, it appears to include a number of window resonances, indicating strong interference between the resonant states and the nonresonant background. This effect was not visible for the $3s^2\,{}^1S\rightarrow 3s3p\,{}^3P$ transition because of the relative weakness of the background cross section. We have also determined differential and partial cross sections for this transition, and values of the partial-cross-section fractions at 90° and 130° for five energies in the threshold region are given in the middle portion of Table IV. Again, the angular distributions vary significantly throughout the resonance region, although not quite as dramatically as in the case of the transition from the ground state to the $3s3p\,{}^3P$ term.

In any experiment on Si^{2+}, a certain fraction of ions will be in the $3s3p\,{}^3P$ metastable state. For that reason, we also calculated the total cross section for the $3s3p\,{}^3P\rightarrow 3s3p\,{}^1P$ spin-forbidden transition, and it is shown in Fig. 5. Although the cross section is smaller than for the other two transitions, it is completely dominated by a strong resonance structure, and a measurement of the cross section for this transition would provide an interesting test of the accuracy of the theoretical calculation. However, as can be seen from the bottom portion of Table IV, the variation in the angular distribution of electrons for this transition is significant, and although it is somewhat less pronounced than for the other two transitions, this would still provide a special challenge to such a measurement.

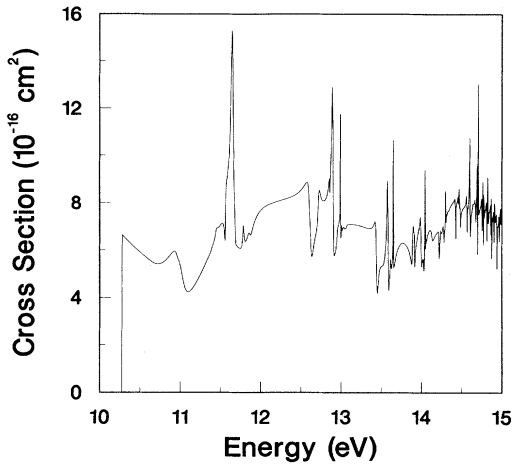

FIG. 4. Cross section for the $3s^2\,{}^1S\rightarrow 3s3p\,{}^1P$ excitation in Si^{2+} from a 12-state R-matrix close-coupling calculation.

As part of extensive distorted-wave calculations for Mg-like ions, Christensen, Norcross, and Pradhan [22] determined collision strengths for transitions between a number of lower-lying levels of Ar^{6+}. In these calculations some of the resonance contributions were included by using quantum-defect theory and by including bound channels in the $(N+1)$-electron expansion. We have carried out R-matrix close-coupling calculations for Ar^{6+} in order to determine the cross sections for the three transitions discussed above for Si^{2+}. However, in this case, the $3s4s$ and $3s4p$ configurations are higher in energy, and comparable accuracy can be achieved from an 8-state, rather than a 12-state, calculation.

In Table V, we show the calculated energies of the eight terms included in the close-coupling expansion in comparison to experiment [20]. All the orbitals in this

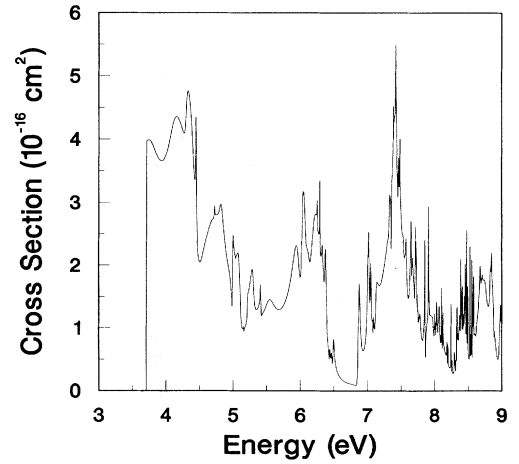

FIG. 5. Cross section for the $3s3p\,{}^3P\rightarrow 3s3p\,{}^1P$ excitation in Si^{2+} from a 12-state R-matrix close-coupling calculation.

TABLE V. Energies (eV) for the terms included in the 8-state close-coupling expansion in Ar^{6+} relative to the $3s^2\,{}^1S$ ground state. The $1s$, $2s$, $2p$, and $3s$ orbitals were determined from a SCHF calculation for the term $3s^2\,{}^1S$, while the $3p$ and $3d$ orbitals were determined from SCHF calculations for the terms $3s3p\,{}^1P$ and $3s3d\,{}^1D$, respectively, with all other orbitals frozen. The configuration-interaction expansions included the six terms $3p3d\,{}^3P$, $3d^2\,{}^3P$, $3p3d\,{}^1P$, $3d^2\,{}^1S$, and $3d^2\,{}^1D$ in addition to the eight terms listed below.

Number	Term	Theory	Experiment (Ref. [20])
1	$3s^2\,{}^1S$	0.00	0.00
2	$3s3p\,{}^3P$	13.78	14.07
3	$3s3p\,{}^1P$	21.20	21.17
4	$3p^2\,{}^1D$	32.16	32.82
5	$3p^2\,{}^3P$	33.11	33.57
6	$3p^2\,{}^1S$	39.13	
7	$3s3d\,{}^3D$	39.98	40.07
8	$3d3d\,{}^1D$	46.62	45.91

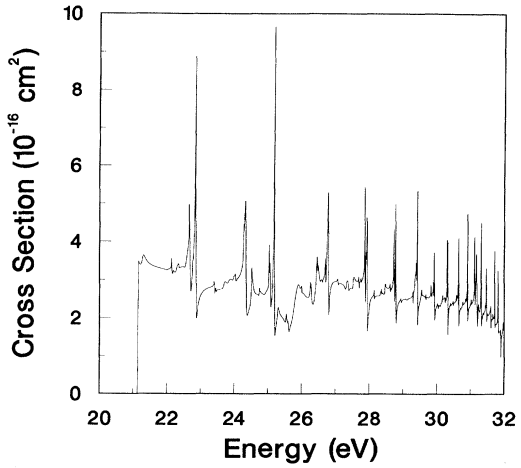

FIG. 7. Cross section for the $3s^2\,{}^1S \rightarrow 3s3p\,{}^1P$ excitation in Ar^{6+} from an 8-state R-matrix close-coupling calculation.

calculation were spectroscopic and were determined from SCHF calculations. The configuration-interaction expansions included the six terms listed above the table, in addition to the eight terms included in the close-coupling expansion.

The R-matrix calculations were performed in a way similar to that described above for Si^{2+}. The total cross sections for the $3s^2\,{}^1S \rightarrow 3s3p\,{}^3P$, $3s^2\,{}^1S \rightarrow 3s3p\,{}^1P$, and $3s3p\,{}^3P \rightarrow 3s3p\,{}^1P$ transitions are shown in Figs. 6, 7, and 8, respectively. As can be seen, the spin-forbidden transitions are again dominated by a complex resonance structure. In the case of the dipole-allowed transition shown in Fig. 7, the pronounced window resonances indicate that interference between the resonant states and the nonresonant background is still quite strong in this six-times-ionized species.

From the 8-state calculation in Ar^{6+}, we also determined differential cross sections and partial-cross-section fractions for these three transitions; we found that the variation in the angular distribution of electrons, within the resonance regions for this ion, is similar to that discussed above for Si^{2+}. However, it is also interesting to consider how this angular distribution changes between different kinds of transitions, with respect to the nonresonant background cross section.

It would be very difficult to identify the background contribution from the results of the 8-state calculation because of the dominance of the resonance structures. For this reason, we performed simple 2-state calculations for the $3s^2\,{}^1S \rightarrow 3s3p\,{}^1P$ dipole-allowed transition and the $3s^2\,{}^1S \rightarrow 3s3p\,{}^3P$ spin-forbidden transition, since such calculations cannot include any resonant contributions. However, these should be considered model calculations for the nonresonant contributions only and are not intended to provide accurate angular distributions for these

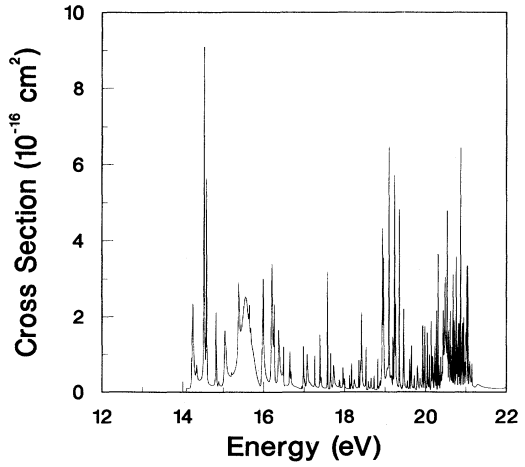

FIG. 6. Cross section for the $3s^2\,{}^1S \rightarrow 3s3p\,{}^3P$ excitation in Ar^{6+} from an 8-state R-matrix close-coupling calculation.

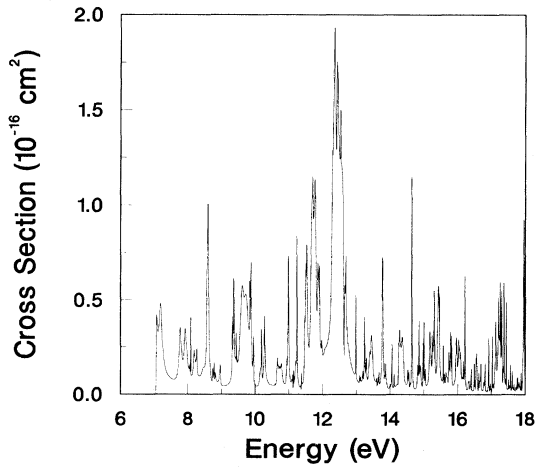

FIG. 8. Cross section for the $3s3p\,{}^3P \rightarrow 3s3p\,{}^1P$ excitation in Ar^{6+} from an 8-state R-matrix close-coupling calculation.

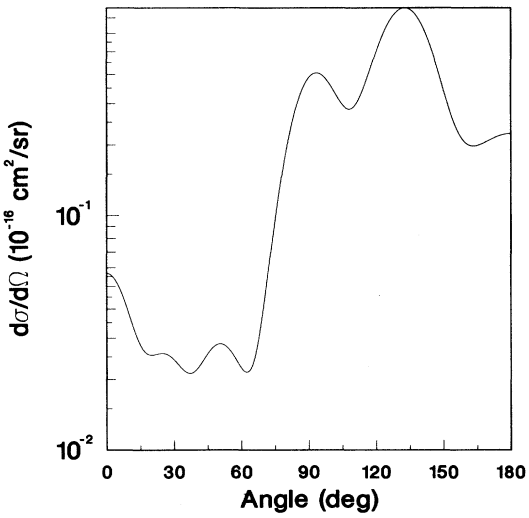

FIG. 9. Angular differential cross section corresponding to the nonresonant contribution to the $3s^2\,{}^1S \rightarrow 3s3p\,{}^1P$ excitation in Ar^{6+} from a 2-state R-matrix close-coupling calculation at an energy of 1.05 times the threshold energy.

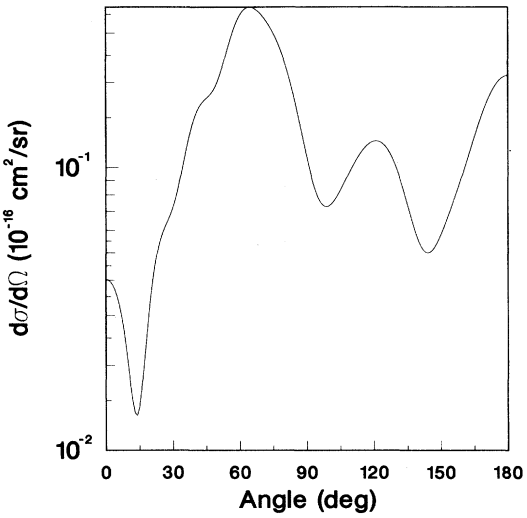

FIG. 11. Angular differential cross section corresponding to the nonresonant contribution to the $3s^2\,{}^1S \rightarrow 3s3p\,{}^1P$ excitation in Ar^{6+} from a 2-state R-matrix close-coupling calculation at an energy of 2.00 times the threshold energy.

transitions. The differential cross section for the dipole-allowed transition at 1.05 times the threshold energy is shown in Fig. 9. This is accompanied by a plot of the partial-cross-section fraction in Fig. 10. As can be seen from these plots, the electrons are preferentially back-scattered near threshold with less than 20% of the electrons scattered in the forward direction.

This type of angular distribution near threshold was first observed in the differential cross section for the $3s \rightarrow 3p$ excitation in Ar^{7+}. We performed that particular calculation in response to indications of significant backscattering in an energy-loss experiment for this transition in Ar^{7+} by Guo *et al.*, which has now been confirmed with further measurements by that same group [23]. In that case, partial-cross-section-fraction calculations indicated that less than 10% of the electrons are scattered in the forward direction. Our differential-cross-section calculation was performed using scattering matrices generated from earlier 7-state R-matrix calculations [24] at energies where the resonant contributions

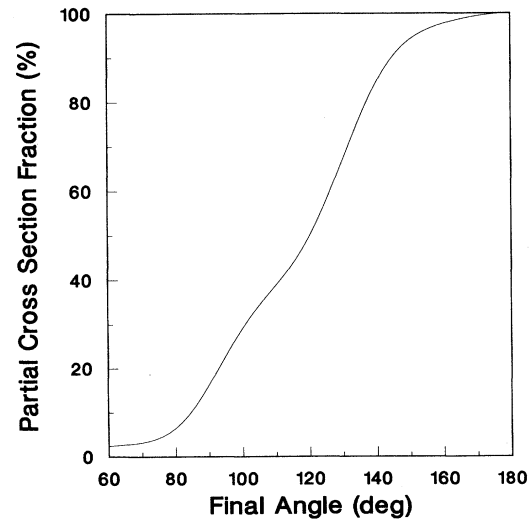

FIG. 10. Partial-cross-section fraction corresponding to the nonresonant contribution to the $3s^2\,{}^1S \rightarrow 3s3p\,{}^1P$ excitation in Ar^{6+} from a 2-state R-matrix close-coupling calculation at an energy of 1.05 times the threshold energy.

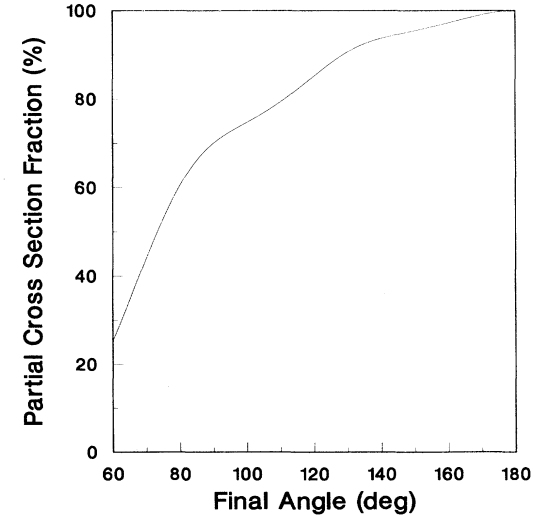

FIG. 12. Partial-cross-section fraction corresponding to the nonresonant contribution to the $3s^2\,{}^1S \rightarrow 3s3p\,{}^1P$ excitation in Ar^{6+} from a 2-state R-matrix close-coupling calculation at an energy of 2.00 times the threshold energy.

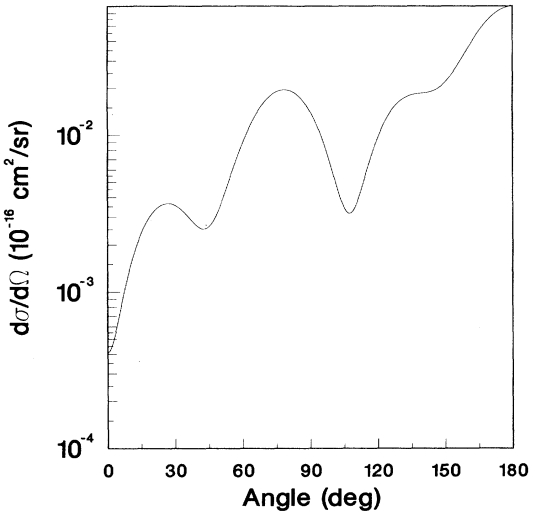

FIG. 13. Angular differential cross section corresponding to the nonresonant contribution to the $3s^2\,{}^1S \rightarrow 3s3p\,{}^3P$ excitation in Ar^{6+} from a 2-state R-matrix close-coupling calculation at an energy of 1.05 times the threshold energy.

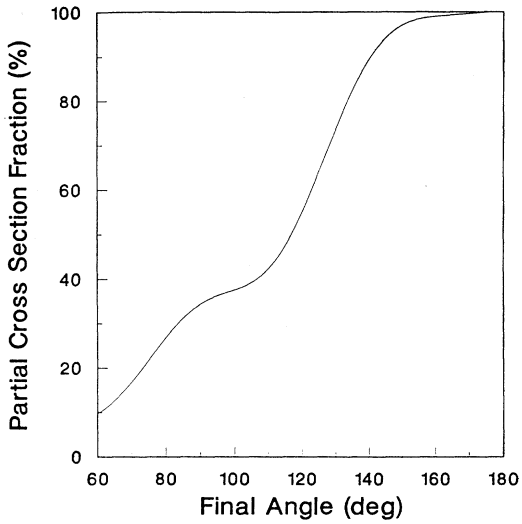

FIG. 15. Angular differential cross section corresponding to the nonresonant contribution to the $3s^2\,{}^1S \rightarrow 3s3p\,{}^3P$ excitation in Ar^{6+} from a 2-state R-matrix close-coupling calculation at an energy of 2.00 times the threshold energy.

were negligible. However, this same behavior was seen in a distorted-wave calculation by Clark [25] and we also performed distorted-wave calculations, with and without exchange, and found the same characteristic backscattering. This indicates that such behavior in the angular distribution near threshold is independent of the effects of continuum coupling and electron exchange.

However, there is theoretical [3,26] and experimental [3] evidence that the electrons are primarily scattered in the forward direction for the $3s \rightarrow 3p$ transition in Ar^{7+} at high electrons energies. This is also true for the dipole-allowed transition in Ar^{6+}. The differential cross section and partial-cross-section fraction from our 2-state calculation for this transition, at twice the threshold energy, are shown in Figs. 11 and 12, respectively. At this energy, the electrons are scattered primarily in the forward direction, with approximately 70% of them scattered at angles less than 90°.

The behavior for spin-forbidden transitions is quite different from that seen for dipole-allowed transitions. The differential cross section and partial-cross-section fraction from our 2-state calculation for the $3s^2\,{}^1S \rightarrow 3s3p\,{}^3P$ transition at 1.05 times the threshold energy are shown in Figs. 13 and 14, respectively. We see

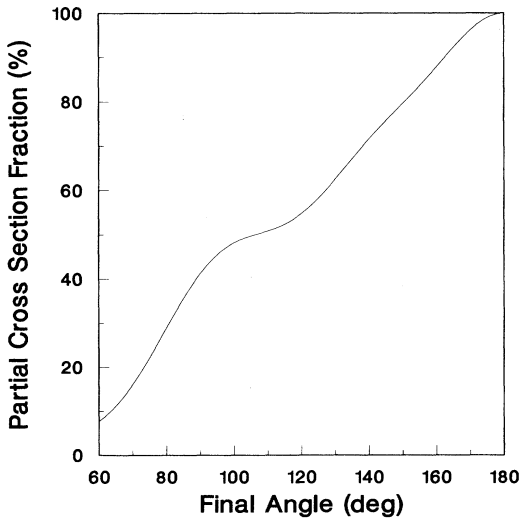

FIG. 14. Partial-cross-section fraction corresponding to the nonresonant contribution to the $3s^2\,{}^1S \rightarrow 3s3p\,{}^3P$ excitation in Ar^{6+} from a 2-state R-matrix close-coupling calculation at an energy of 1.05 times the threshold energy.

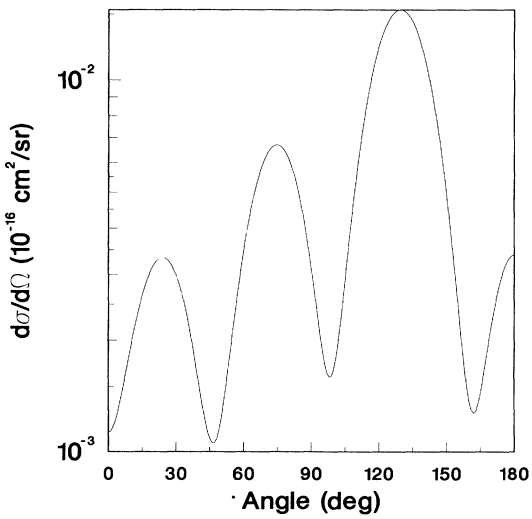

FIG. 16. Partial-cross-section fraction corresponding to the nonresonant contribution to the $3s^2\,{}^1S \rightarrow 3s3p\,{}^3P$ excitation in Ar^{6+} from a 2-state R-matrix close-coupling calculation at an energy of 2.00 times the threshold energy.

that the electrons are not nearly as backscattered as in the case of the dipole-allowed transition, with just over 40% of the electrons scattered in the forward direction. Similar plots at twice the threshold energy are shown in Figs. 15 and 16. At this energy, the electrons are not nearly as forward scattered as in the case of the dipole-allowed transitions, with just over 30% scattered through angles less than 90°. However, this angular distribution may be difficult to observe experimentally; the nonresonant contribution to the cross section is relatively weak, and, as discussed above, the resonant contribution, which dominates in the threshold region, will change the angular distribution significantly.

IV. SUMMARY

We have carried out total and angular differential-cross-section calculations for the $3s^2\,{}^1S \rightarrow 3s3p\,{}^3P$, $3s^2\,{}^1S \rightarrow 3s3p\,{}^1P$, and $3s3p\,{}^3P \rightarrow 3s3p\,{}^1P$ excitations in Si^{2+} and Ar^{6+} at low electron energies, using the close-coupling R-matrix method. For the two spin-forbidden transitions, the cross sections are dominated by the resonance contributions; although not as dominant, these resonances are also important for the dipole-allowed excitation. The differential cross sections and the partial-cross-section fractions are found to be strongly affected by the autoionizing resonance structures.

The final-state electrons corresponding to the nonresonant contributions to the dipole-allowed transition from the ground state in Ar^{6+} were found to be preferentially backscattered at low energies, although the number of electrons forward scattered increases dramatically with energy; this behavior is similar to that found earlier for Ar^{7+}. The spin-forbidden transition from the ground state shows a quite different angular distribution as a function of energy.

Further studies of electron-ion collisions which focus on the angular distribution of scattered electrons are not only important for a better understanding of the physical processes involved, but are also necessary to help plan and interpret possible excitation measurements, in which the scattered electrons are collected. In the future we plan to extend our calculations to heavier ions in the Mg-like isoelectronic sequence.

ACKNOWLEDGMENTS

We would like to thank Dr. Gordon Dunn of JILA for supplying us with the experimental results on Ar^{7+} prior to publication, and the members of the Opacity Project for supplying us with their R-matrix programs. This work was supported by the Office of Fusion Energy, U.S. Department of Energy, under Contract No. DE-AC05-841OR21400 with Martin Marietta Energy Systems, Inc. and Contract No. DE-FG05-86ER53217 with Auburn University.

[1] A. Chutjian, A. Z. Msezane, and R. J. W. Henry, Phys. Rev. Lett. **50**, 1357 (1983).
[2] I. D. Williams, A. Chutjian, and R. J. Mawhorter, J. Phys. B **19**, 2189 (1986).
[3] B. A. Huber, C. Ristori, P. A. Hervieux, M. Maurel, C. Guet, and H. J. Andrä, Phys. Rev. Lett. **67**, 1407 (1991).
[4] E. K. Wahlin, J. S. Thompson, G. H. Dunn, R. A. Phaneuf, D. C. Gregory, and A. C. H. Smith, Phys. Rev. Lett. **66**, 157 (1991).
[5] S. J. Smith, K. F. Man, R. J. Mawhorter, I. D. Williams, and A. Chutjian, Phys. Rev. Lett. **67**, 30 (1991).
[6] See, for example, *Proceedings of the Seventeenth International Conference on the Physics of Electronic and Atomic Collisions, Invited Papers,* edited by W. R. MacGillivray, I. E. McCarthy, and M. C. Standage (Hilger, Bristol, 1992).
[7] Y. Itikawa and K. Sakimoto, Phys. Rev. A **38**, 664 (1988).
[8] A. W. Pangantiwar and R. Srivastava, J. Phys. B **21**, L219 (1988).
[9] D. C. Griffin and M. S. Pindzola, Phys. Rev. A **42**, 248 (1990).
[10] S. Nakazaki and K. A. Berrington, Phys. Rev. A **43**, 3509 (1991).
[11] K. L. Baluja, P. G. Burke, and A. E. Kingston, J. Phys. B **13**, L543 (1980).
[12] G. H. Dunn and R. A. Phaneuf (private communication).
[13] P. G. Burke and W. D. Robb, Adv. At. Mol. Phys. **11**, 143 (1975).
[14] K. A. Berrington, P. G. Burke, K. Butler, M. J. Seaton, P. J. Storey, K. T. Taylor, and Y. Yan, J. Phys. B **20**, 6379 (1987).
[15] C. F. Fischer, Comput. Phys. Commun. **64**, 369 (1991).
[16] S. A. Salvini, Comput. Phys. Commun. **64**, 369 (1991).
[17] K. L. Baluja, P. G. Burke, and A. E. Kingston, J. Phys. B **14**, 1333 (1981).
[18] K. L. Baluja and A. Hibbert, J. Phys. B **13**, L327 (1980).
[19] G. A. Victor, R. F. Stewart, and C. Laughlin, Astrophys. J. Suppl. Ser. **31**, 237 (1976).
[20] C. E. Moore, *Atomic Energy Levels,* Natl. Bur. Stand. (U.S.) Circ. No. 35 (U.S. GPO, Washington, DC, 1971), Vol. 1.
[21] V. M. Burke and M. J. Seaton, J. Phys. B **19**, L527 (1986).
[22] R. B. Christensen, D. W. Norcross, and A. K. Pradhan, Phys. Rev. A **34**, 4704 (1986).
[23] X. Q. Guo, E. W. Bell, J. S. Thompson, G. H. Dunn, M. E. Bannister, R. A. Phaneuf, and A. C. H. Smith, Submitted Phys. Rev. A. **47**, R9 (1993).
[24] N. R. Badnell, M. S. Pindzola, and D. C. Griffin, Phys. Rev. A **43**, 2250 (1990).
[25] R. E. H. Clark (private communication).
[26] M. S. Pinzola, D. C. Griffin, and N. R. Badnell, in *Seventeenth International Conference on the Physics of Electronic and Atomic Collisions, Abstracts of Contributed Papers for Brisbane, Australia, 1991,* edited by I. E. McCarthy, W. R. MacGillivray, and M. S. Standage (Griffith University, Brisbane, 1991), p. 285.